Electronic Supplementary Information (ESI)

Crystallisation of a salt hydrate with a complex solid form landscape

Eszter Tieger[1,2*], Violetta Kiss[3], György Pokol[1], Zoltán Finta[4]

[1]Department of Inorganic and Analytical Chemistry, Budapest University of Technology and Economics, Szt. Gellért tér 4, 1111 Budapest, Hungary, tiegereszter@gmail.com

[2] Zentiva – a Sanofi company, U kabelovny 130, 102 37, Prague, Czech Republic

[3]Janssen Pharmaceuticals, Inc. - Pharmaceutical Companies of Johnson & Johnson, Turnhoutseweg 30, B-2340 Beerse, Belgium

[4]Chinoin Zrt., Tó utca 1-5., 1045 Budapest, Hungary

XRPD

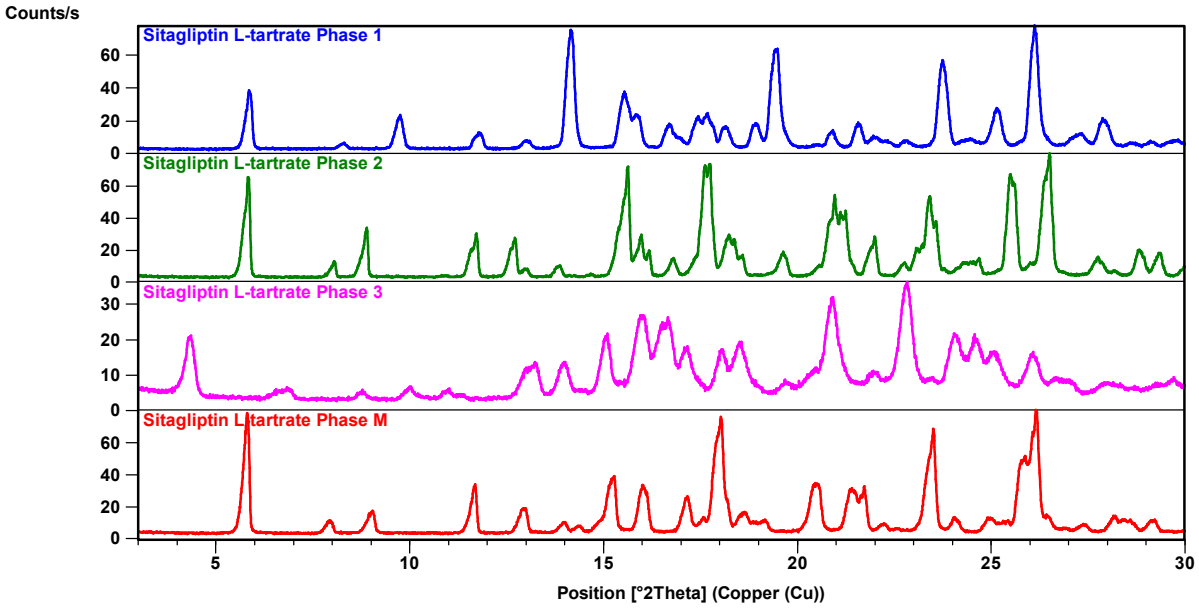

Figure 1. XRPD patterns of the SLT hydrates[1]

[1] E. Tieger, V. Kiss, Gy. Pokol, Z. Finta, M. Dušek, J. Rohlíček, E. Skořepová, Studies on the crystal structure and arrangement of water in sitagliptin L-tartrate hydrates, CrystEngComm, 2016,18, 3819-3831

Variable-humidity X-ray Powder Diffraction (VH-XRPD)

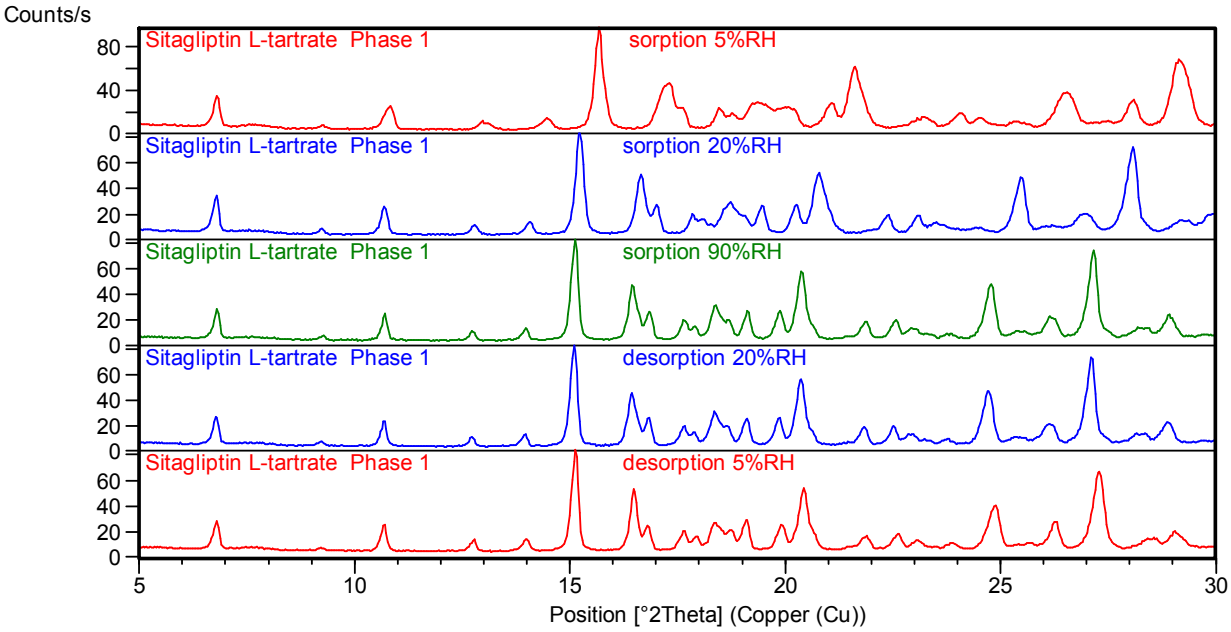

Figure 2. VH-XRPD patterns of Phase 1 at various relative humidity values[1]

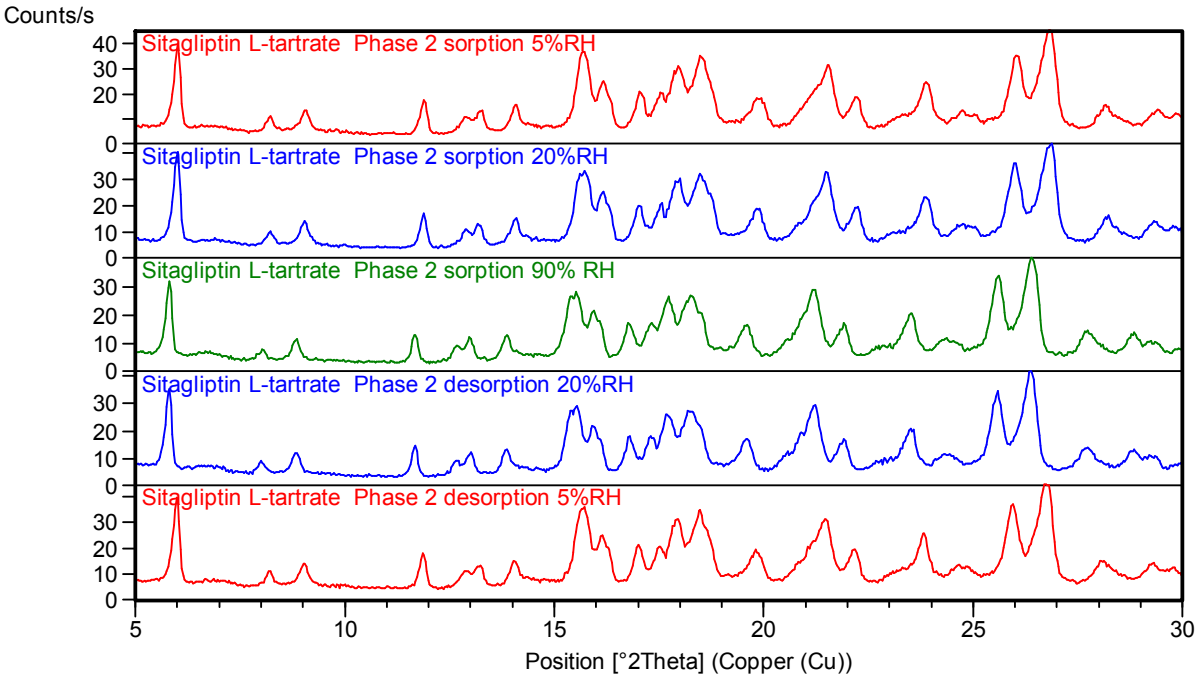

Figure 3. VH-XRPD patterns of Phase 2 at various relative humidity values[1]

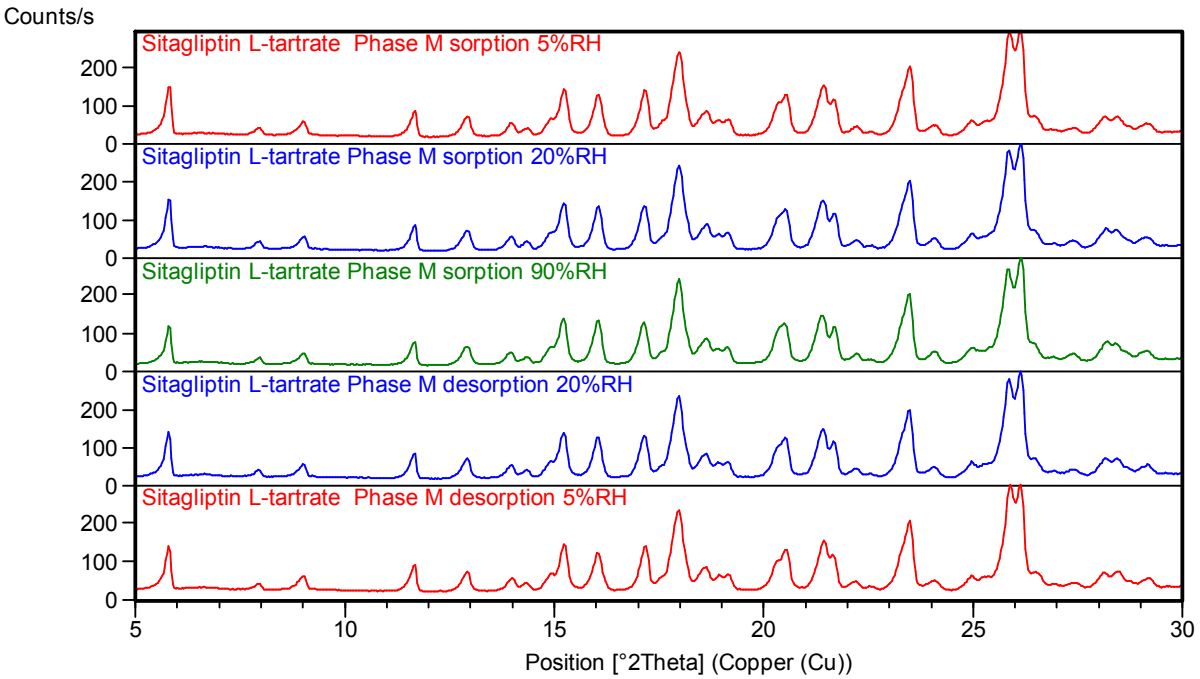

Figure 4. VH-XRPD patterns of Phase M at various relative humidity values[1]

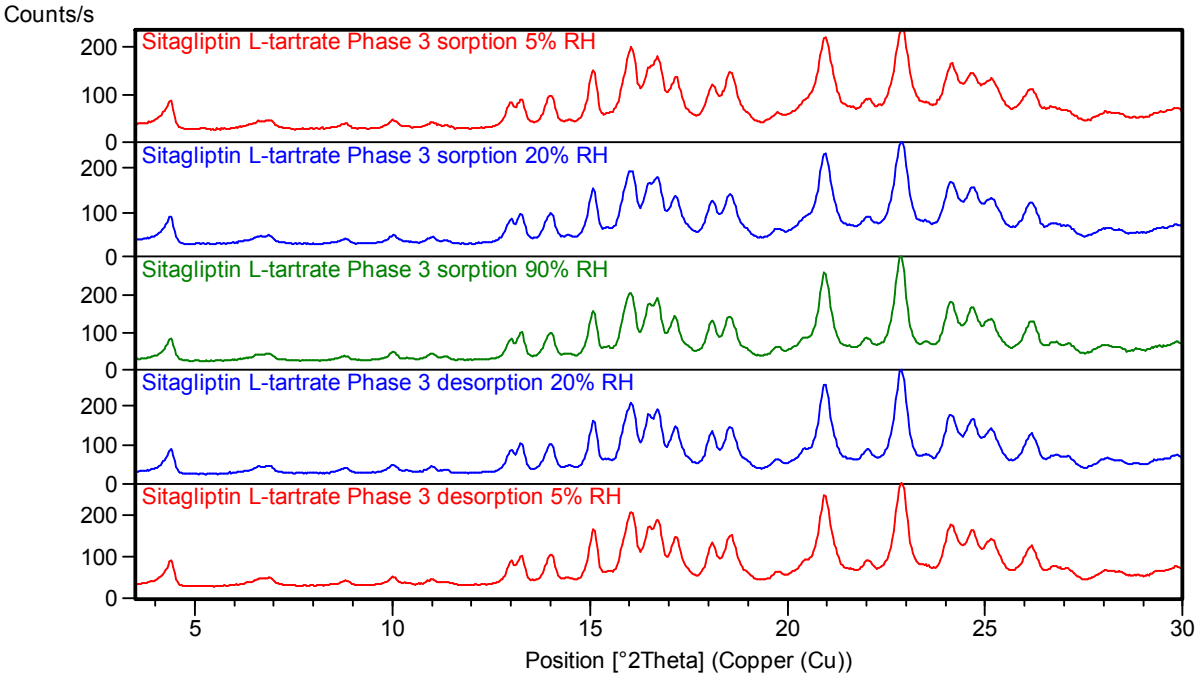

Figure 5. VH-XRPD patterns of Phase 3 at various relative humidity values[1]

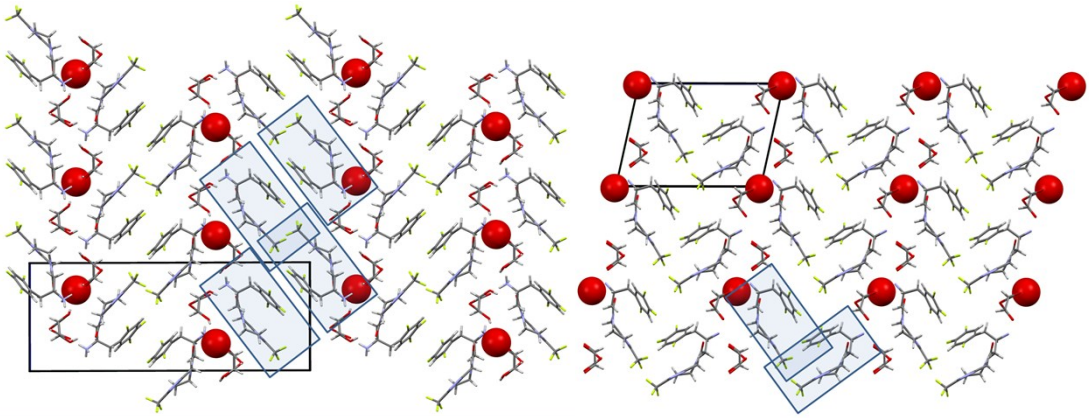

Figure 6. Packing motif of SLT Phase 1 (left) and Phase 2 (right)
Water-O atoms atoms are presented in spacefill style[1]

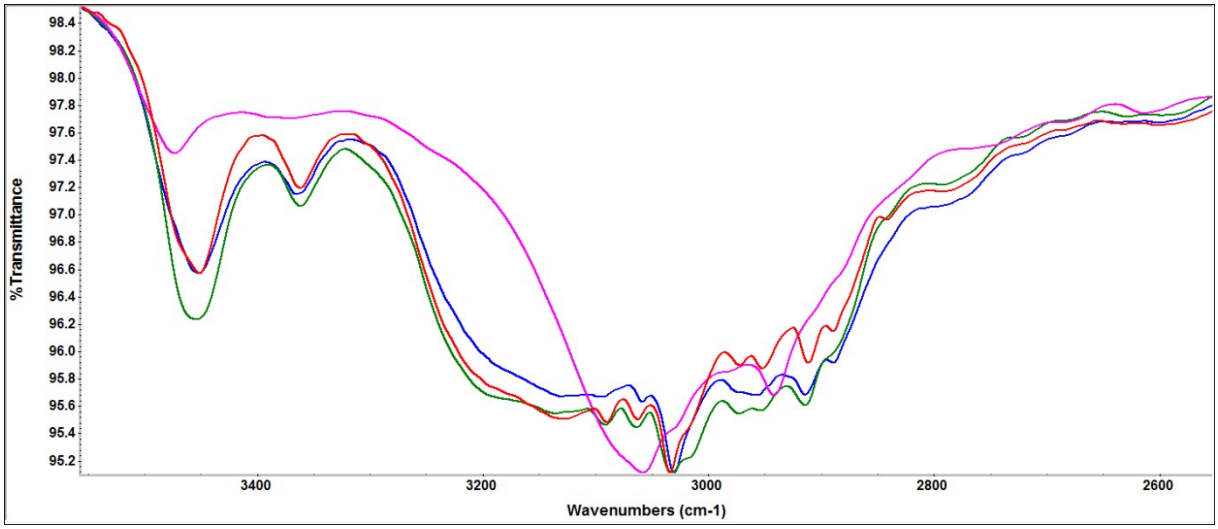

Figure 7. IR spectra of SLT **Phase 1**, **Phase 2**, **Phase 3** and **Phase M** - CH region[1]

Solubility curves

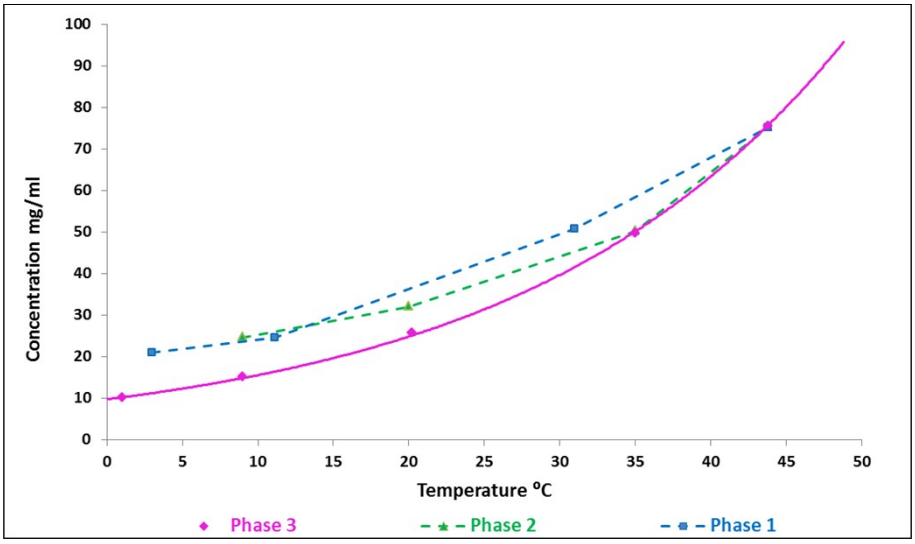

Figure 8. Kinetic solubility of SLT forms in acetone-water 8-2 V/V mixture

In aceton-water 8-2 V/V mixture SLT Phase 3 has the lowest solubility (Figure 8). SLT Phase 1 and Phase 2 started to transform to Phase 3 during the measurement. As it is shown in Figure 8, Phase 2 converted faster, at 35°C the measured points of Phase 2 and Phase 3 coincide, while the complete conversion of Phase 1 occurred till 45°C. XRPD analysis of the undissolved residues has confirmed the transformation.

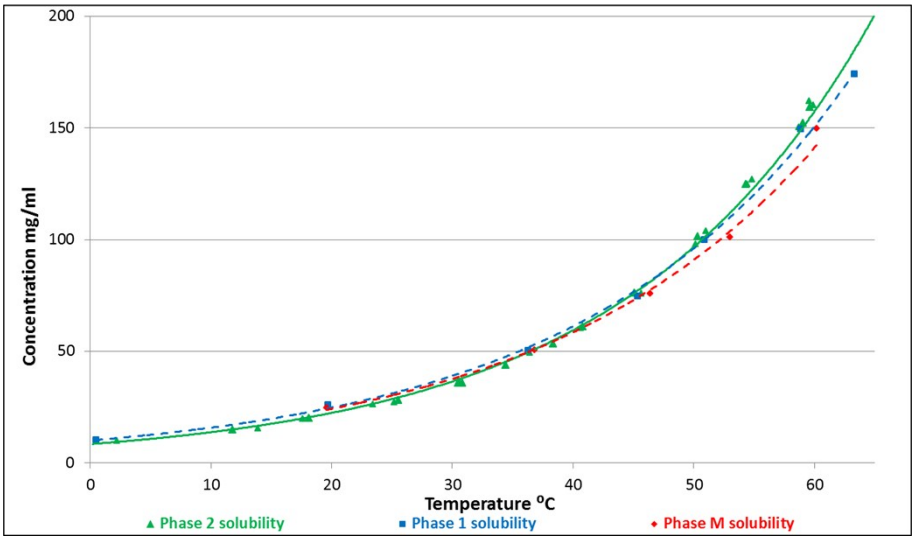

Figure 9. Kinetic solubility of SLT forms in methanol-water 6-4 V/V mixture

In methanol-water 6-4 V/V mixture SLT Phase 2 has the lowest solubility (Figure 9). SLT Phase 2 and Phase M transformed to Phase 2 during the measurement. As it is shown in Figure 9, the solubility curves coincide and XRPD analysis of the undissolved residues has confirmed the transformation.

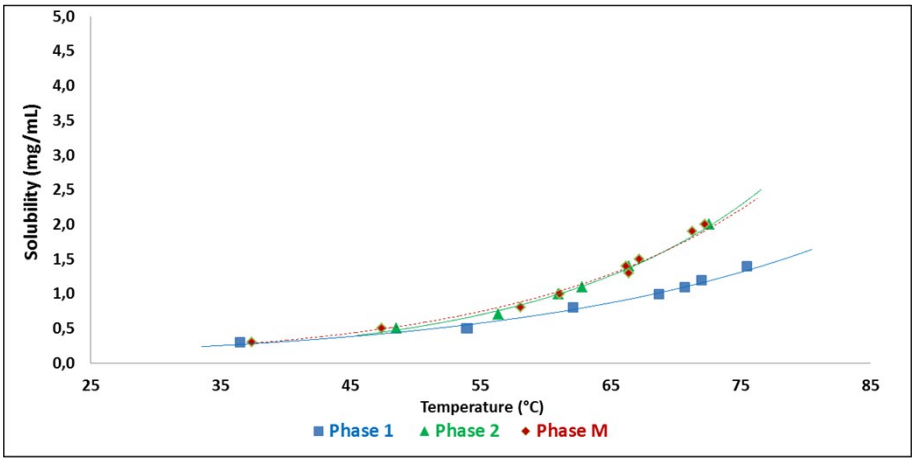

Figure 10. Kinetic solubility of SLT forms in 2-propanol

As it is shown in Figure 8-10 the solubility order of SLT hemihydrates changes according to the solvent media. In acetone-water 8-2 V/V mixture Phase 3 has the lowest solubility, in methanol-water 6-4 V/V mixture Phase 2 has the lowest solubility and in 2-propanol Phase 1 has the lowest solubility. These results are consistent with the outcome of the solvent mediated polymorphic transformations. According to Figure 10, the SLT forms has poor solubility in pure 2-propanol, which could explain the presence of mixtures in the suspensions at lower temperatures.

Equilibrium Solubility determination - shake flask method

Equilibrium solubility measurements were performed by agitating excess amounts of the appropriate forms in 10 mL of solvent in thermostated water baths. After equilibration times of 24 h at 40, 60 and 75°C and 168 h at 0 and 20°C, the phases were separated and the concentration was determined gravimetrically. Assays were performed in triplicate. The final crystal form of the residual solids was confirmed by XRPD. Phase 2 was stable up to 40°C, above which transformed to Phase 1, while Phase 3 transformed to Phase 1 above 0°C.

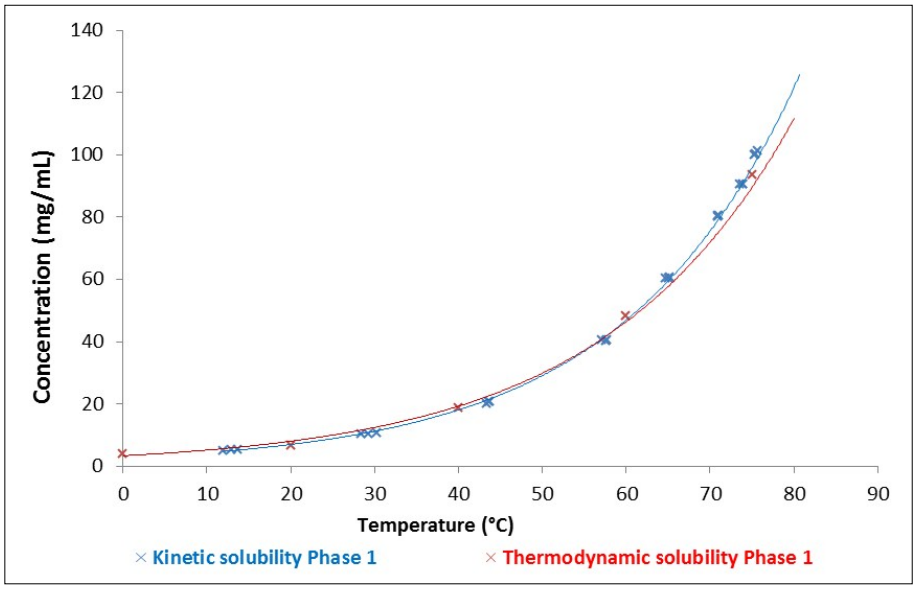

Figure 11. Kinetic and thermodynamic solubility of SLT Phase 1 in 2-propanol-water 8-2 V/V mixture

The kinetic and thermodynamic solubility curve of Phase 1 in 2-propanol-water 8-2 V/V mixture are in good agreement (Figure 11).

ATR-FTIR

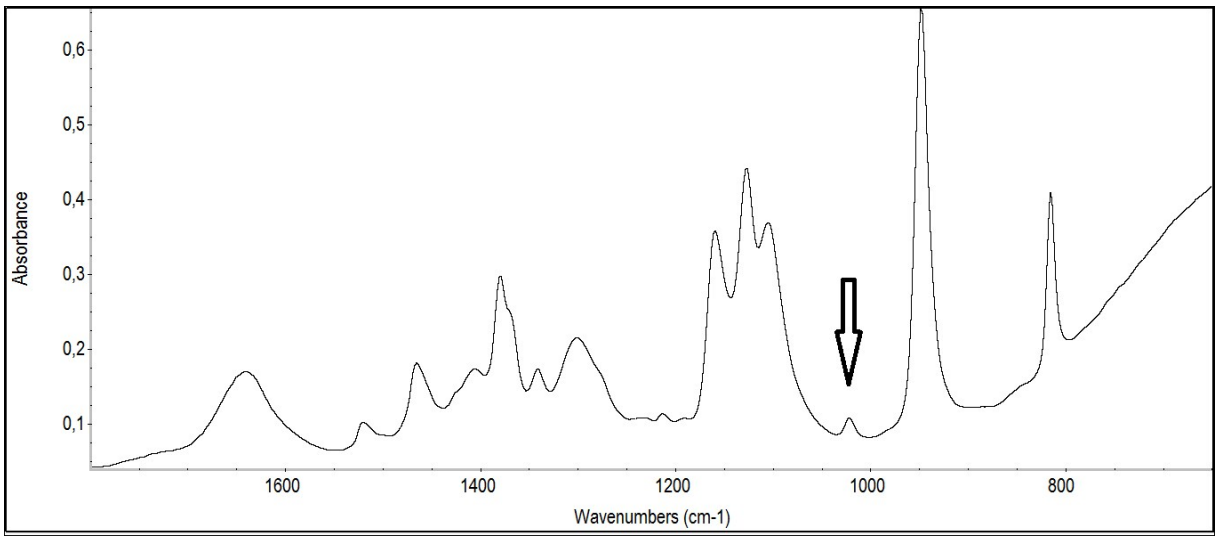

Figure 12. IR spectrum of SLT in 2-propanol-water 8-2 V/V mixture, the applied peak is marked with an arrow

As shown in Figure 12, SLT produces a distinct FTIR fingerprint in 2-propanol-water 8-2 V/V mixtures, with few peaks available for concentration assessment. Different peaks were tested, and it was determined that the peak at 1022 cm^{-1} provides good results in terms of reproducibility and accuracy, so the spectrum range of this band was chosen for the study. Baseline correction was applied to compensate for the temperature effect. In order to obtain a

calibration model that is applicable over a wide range of process conditions, an extensive calibration set was designed including samples in under- as well as in supersaturated regions (Figue 13). According to Figure 13 the temperature has only slight influence on the absorbance and temperature correction was not vital.

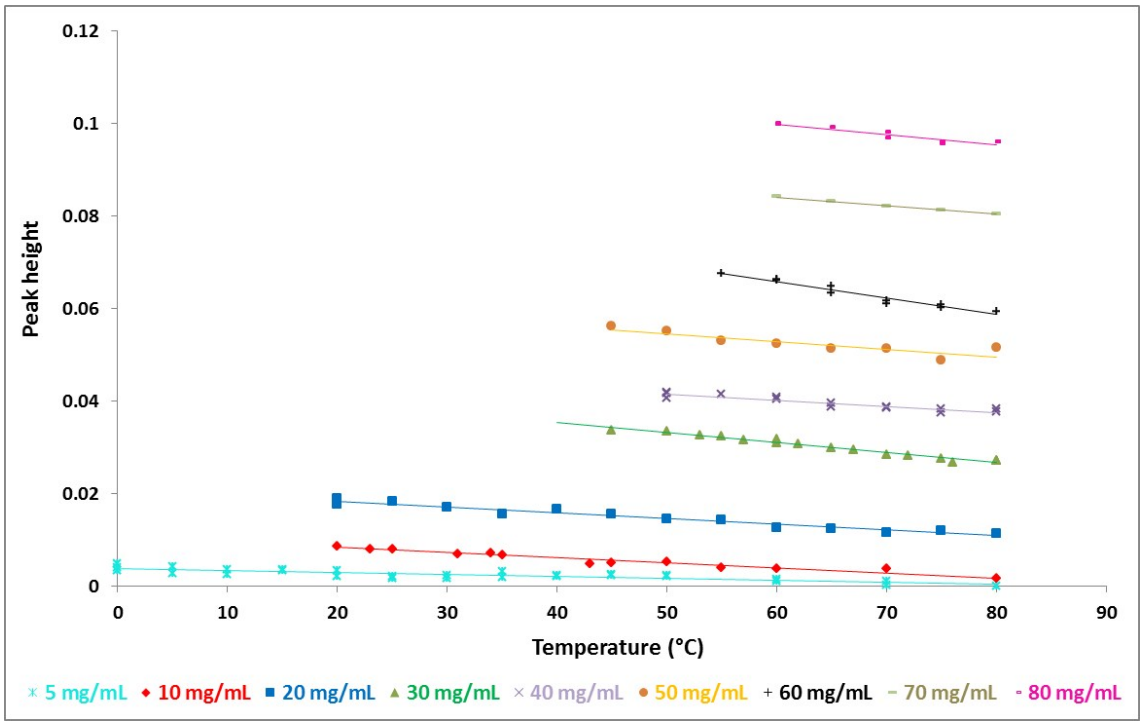

Figure 13. Absorbance of SLT solutions at 1006.6-1033.3 cm^{-1} of constant concentrations at different temperatures

Details of the CLS calibration:

Number of samples: 16 calibration spectra, 2 validation spectra

Applied spectrum range: 1006.6-1033.3 cm^{-1}

Baseline type: two points: 1004.7-1006.6 and 1033.3-1035.6 cm^{-1}, minimum in range

Concentration range: 0-80 mg/mL

RMSEC= 0.714 and **RMSEP**=0.143

Calibration was performed using various concentrations including spectra of the same concentrations, measured at different temperatures. The spectrum range was applied after baseline correction of the original spectra. Excellent linearity was obtained (Figure 14).

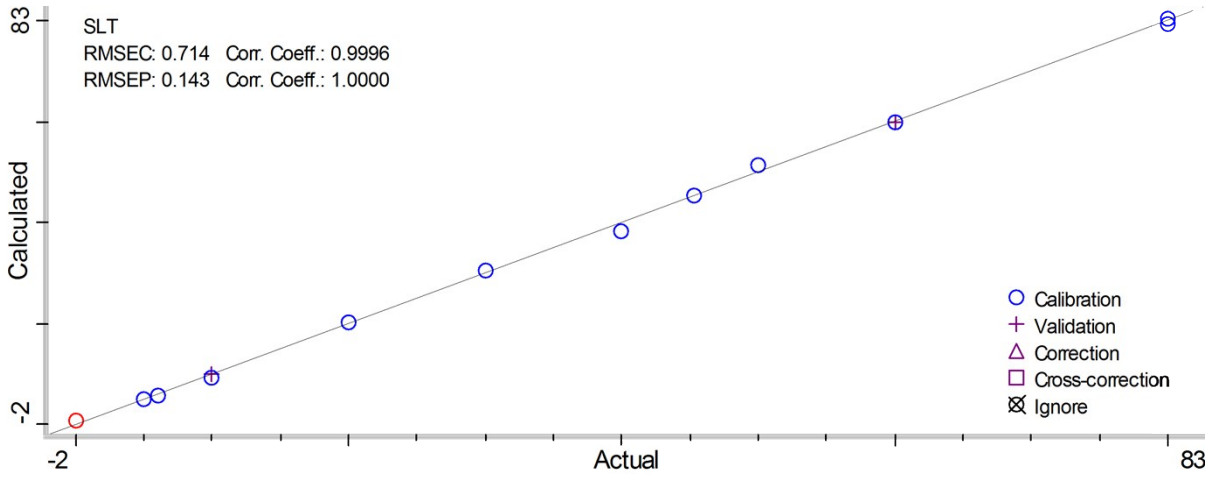

Figure 14. IR calibration curve for SLT: concentration versus spectrum range in the 1006-1033cm $^{-1}$ wavenumber region measured in 2-propanol-water 8-2 V/V mixture

FBRM

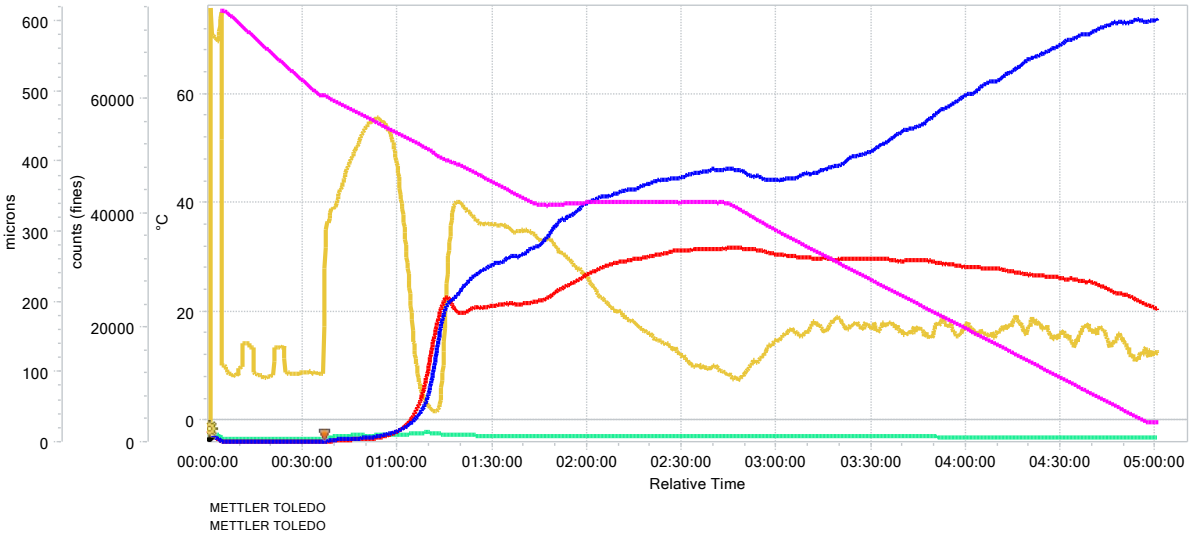

Figure 15. CLD data during crystallisation along with the cooling profile applying 0.5% seed (non sieved, non aged) at 60°C
Counts no Wt<10 µm, no Wt 10-100 µm, , median No wt, Mean Sqr wt

Trend	At the end of the process
counts No Wt <10	75597.38
counts No Wt 10-100	22376.71
Median No Wt	4.91
Mean Sqr Wt	119.14

When 0.5% non sieved, non aged seed was applied at 60°C (σ=28%), the seeding crystals did not dissolve, but could not induce secondary nucleation. Nucleation occurred when the temperature has reached the metastable boundary. Figure 15 shows the evolution of the chord counts during the experiment, measured by the FBRM probe. The nucleation event resulted in

a sudden and steep rise in the chord counts. The results from the in-situ techniques, FBRM and FTIR were consistent with each other. As spontaneous crystallisation occurred at high supersaturation, the resulting needles were really fine and brittle as evidenced by the median chord length: 4.91 µm. The median of the chord length gives an estimation about the average needle width.

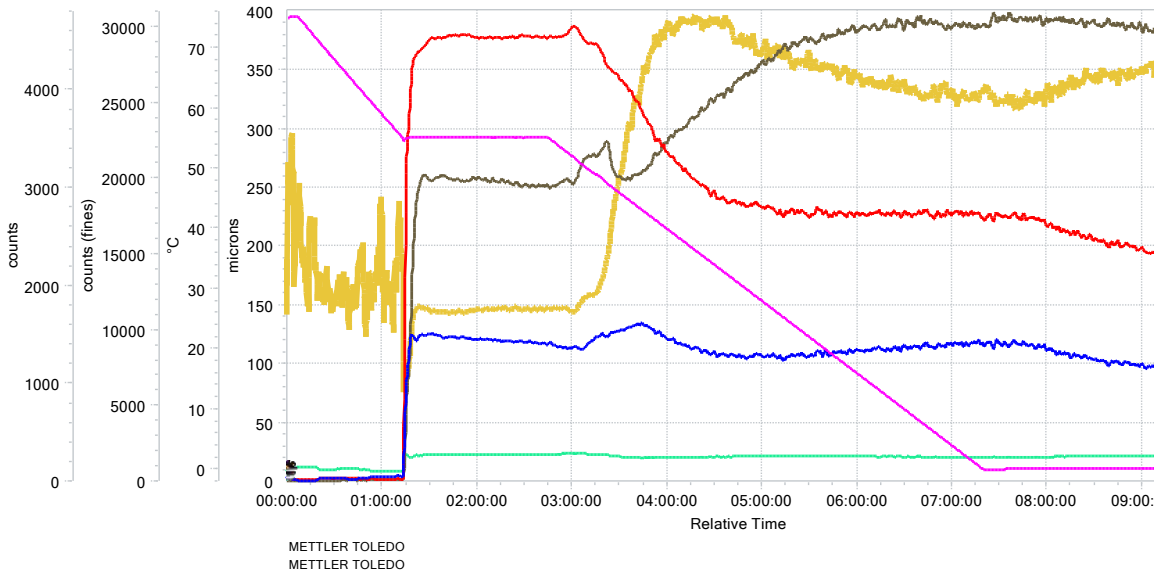

Figure 16. CLD data during crystallisation along with the cooling profile applying 0.5% sieved, aged seed at 55°C followed by an 1 hour isotherm
Temperature, Counts no Wt<10 µm, no Wt 10-100 µm, no Wt 100-1000 µm, median No wt, Mean Sqr wt

Trend	At the end of the process
counts No Wt <10	34011.87
counts No Wt 10-100	25322.31
Median No Wt	8.41
Mean Sqr Wt	340.19

In the process depicted in Figure 16 0.5% sieved, aged seed was applied at 55°C (σ=62.5%), and the seeds were left to mature for 1 h at the seeding temperature before additional cooling was applied. Excessive nucleation occurred which is evidenced by the almost vertical increase in the chord counts. Figure 16 shows the evolution of the chord counts during the experiment, measured by the FBRM probe. The nucleation event resulted in a sudden and steep rise in the chord counts, which during the isotherm could reach equilibrium, the trends became nearly constant. The results from the in-situ techniques, FBRM and FTIR were consistent with each other. The extensive nucleation was seen by the sudden decrease in concentration, measured by the FTIR probe. When the cooling ramp starts, secondary nucleation and agglomeration occurs. The shape of the square-weighted mean CLD distribution is a good indicator of the agglomeration, as it emphasizes the coarse end of the distribution. The square weighted distribution is increasing rapidly and does not decrease significantly till the end of the

process. This indicates that the SLT crystals are aggregating, which was confirmed by analysing the obtained product by scanning electron microscopy (Figure 22). However, the nucleation kinetics were similar to those depicted in Figure 17, the resulting PSD did not meet the specifications leading to a bimodal distribution, as shown in Figure 21.

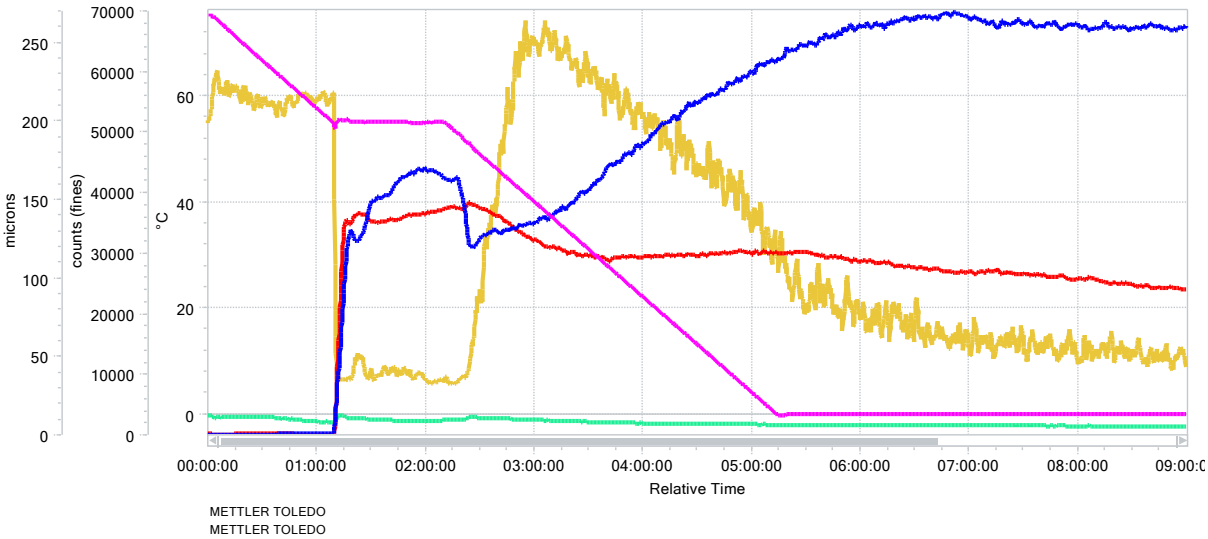

Figure 17. CLD data during crystallisation along with the cooling profile applying 1% sieved, aged seed at 55°C followed by an 1 hour isotherm

Temperature, **Counts** **no Wt<10 µm**, **no Wt 10-100 µm**, **median No wt**, **Mean Sqr wt**

Trend	At the end of the process
counts No Wt <10	64061.48
counts No Wt 10-100	19940.12
Median No Wt	7.06
Mean Sqr Wt	41.01

In the process depicted in Figure 17 1% sieved, aged seed was applied at 55°C (σ=62.5%), and the seeds were left to mature for 1 h at the seeding temperature before additional cooling was applied. Excessive nucleation occurred which is evidenced by the almost vertical increase in the chord counts. Figure 17 shows the evolution of the chord counts during the experiment, measured by the FBRM probe. The nucleation event resulted in a sudden and steep rise in the chord counts. When the cooling ramp starts, secondary nucleation occurs and the interaction of the particles resulted in loosely bound aggregates which easily break up upon further stirring. The square weighted distribution is increasing rapidly but decreased significantly till the end of the process. The resulting PSD met the specifications (Figure 18). Therefore, however the application of 0.5% sieved, aged seed was sufficient to induce extensive nucleation, due to the observed agglomeration, the application of 1% seeds was selected. Double amount of seed resulted in a more significant concentration decrease, thus in lower supersaturation at the end of the isotherm, which mitigated the agglomeration of the fine needles upon further cooling.

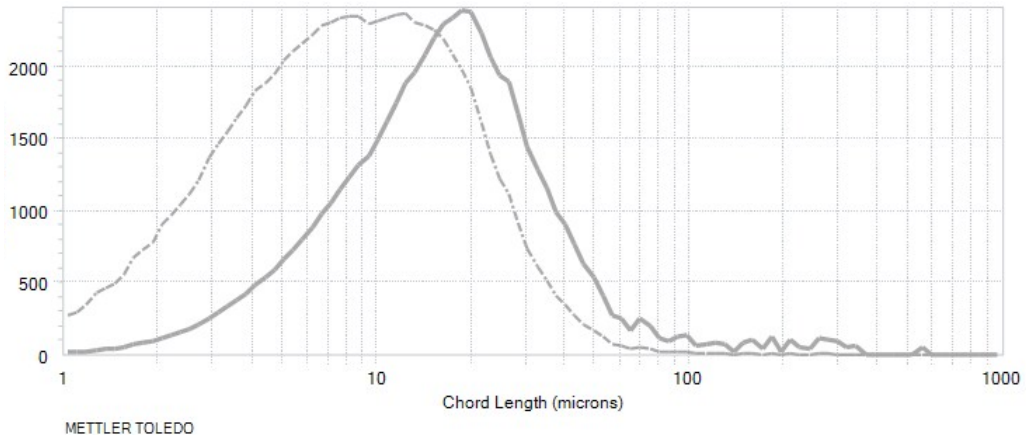

Figure 18. Chord length distributions at the end of the process applying 1% sieved, aged seed: non-weighted distribution (dashed line), square weighted distribution (solid line)

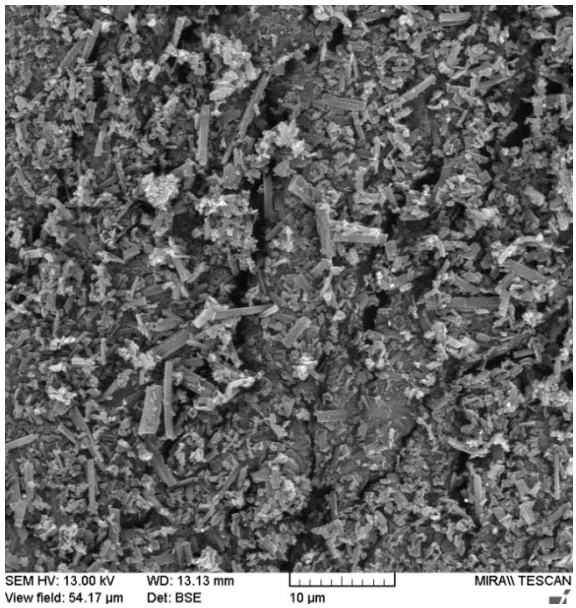

Figure 19. Electron micrograph of the sieved SLT Phase 1 crystals used for seeding

Figure 20. Electron micrograph of a non-agglomerated SLT Phase 1 batch

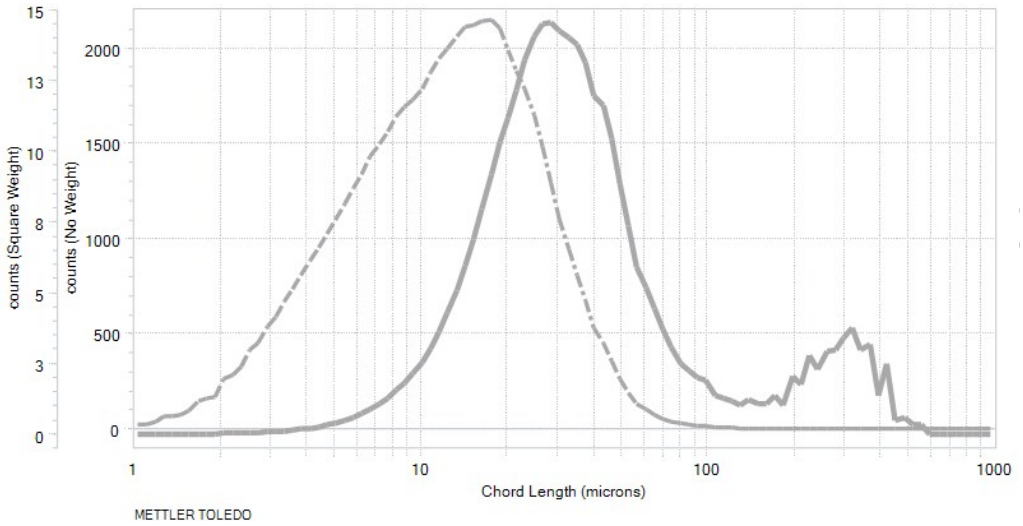

Figure 21. Chord length distribution of an agglomerated SLT Phase 1 batch

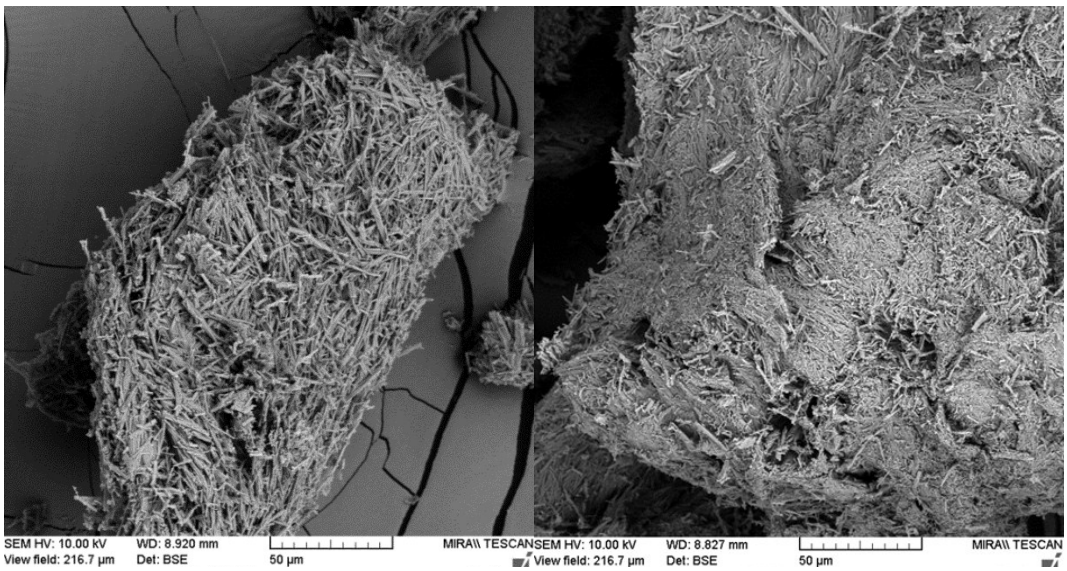

Figure 22. Electron micrographs of an agglomerated SLT Phase 1 batch